Supporting Information for

Boron Nanosheet-Supported Rh Catalysts for Hydrogen Evolution: A New Territory for the Strong Metal-Support Interaction Effect

Keng Chen,[†,¶] Zeming Wang,[†,¶] Liang Wang,[*,†] Xiuzhen Wu,[†] Bingjie Hu,[†] Zheng Liu,[*,§] and Minghong Wu[*,‡,∥]

[†]Institute of Nanochemistry and Nanobiology, School of Environmental and Chemical Engineering, Shanghai University, 99 Shangda Road, BaoShan District, Shanghai 200444, P.R. China

[§]School of Materials Science and Engineering, Nanyang Technological University, 50 Nanyang Avenue, Singapore 639798, Singapore

[‡]Shanghai Applied Radiation Institute, Shanghai University, 333 Nanchen Road, Baoshan District, Shanghai 200444, P.R. China

[∥]Key Laboratory of Organic Compound Pollution Control Engineering (MOE), Shanghai University, Shanghai 200444, P. R. China

[¶]These authors contributed equally to this work.

*E-mail: wangl@shu.edu.cn (L. Wang); Z.Liu@ntu.edu.sg (Z. Liu); mhwu@shu.edu.cn (M. Wu).

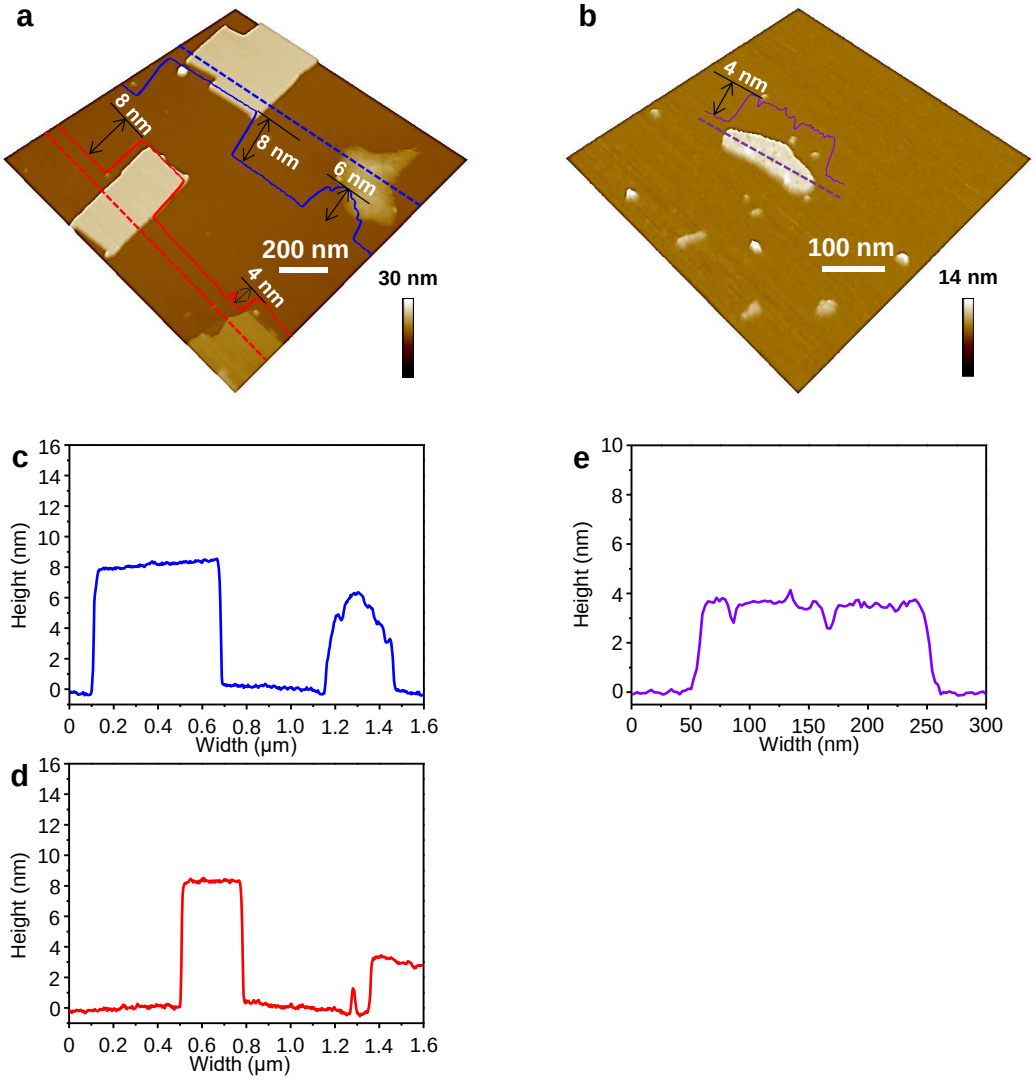

Fig. S1 **a**, **b** Three-dimensional AFM images of BNS and Rh NP@BNS. **c**, **d** The corresponding height profile for BNS. **e** The corresponding height profile for Rh NP@BNS.

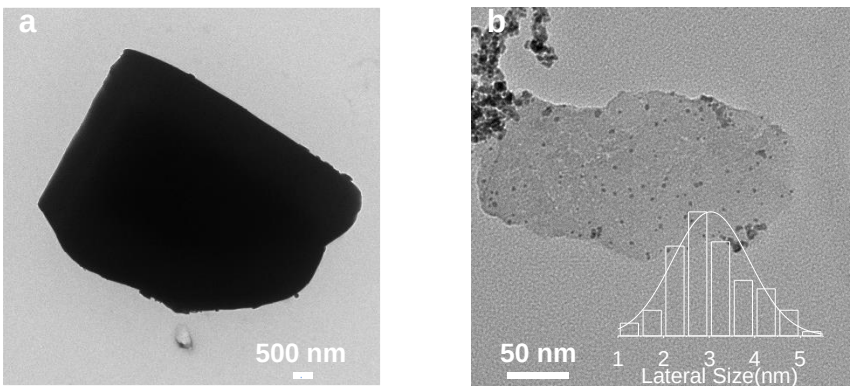

Fig. S2 **a** TEM images of Bulk B. **b** High-resolution TEM images of Rh NP@BNS

(inset: lateral size distribution of Rh NP).

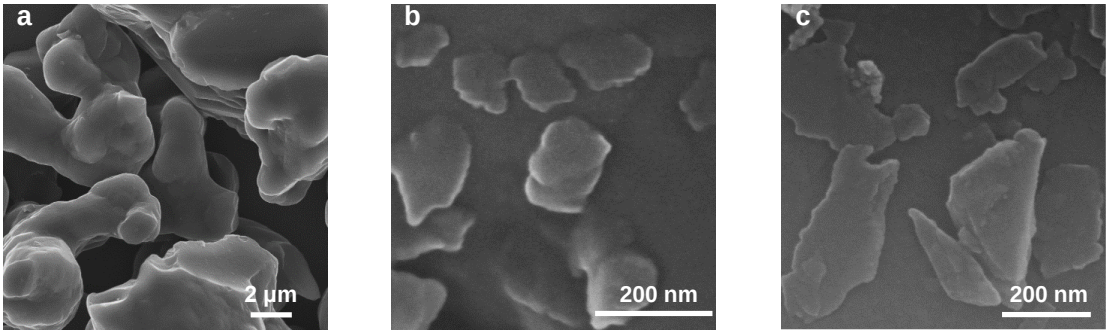

Fig. S3 SEM images of **a** Bulk B, **b** BNS, **c** Rh NP@BNS.

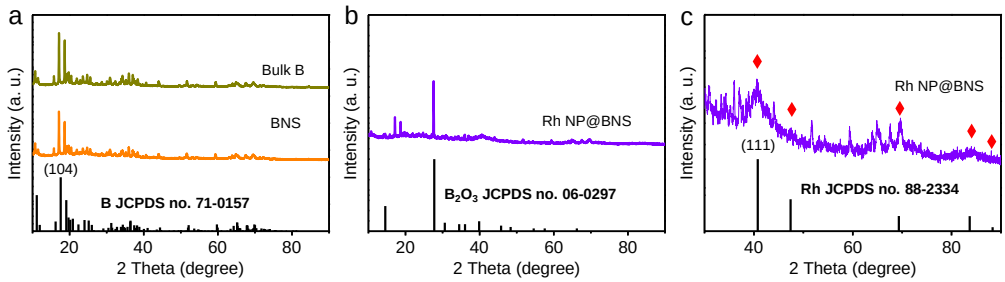

Fig. S4 a XRD patterns of Bulk B and BNS, Matching PDF card (JCPDS No. 71-0157). **b** XRD patterns of Rh NP@BNS, Compare with B_2O_3 PDF card (JCPDS No. 06-0297). **c** The enlarged part of the XRD pattern of Rh NP @ BNS from 30° to 90°, and the corresponding Rh PDF card (JCPDS No. 88-2334).

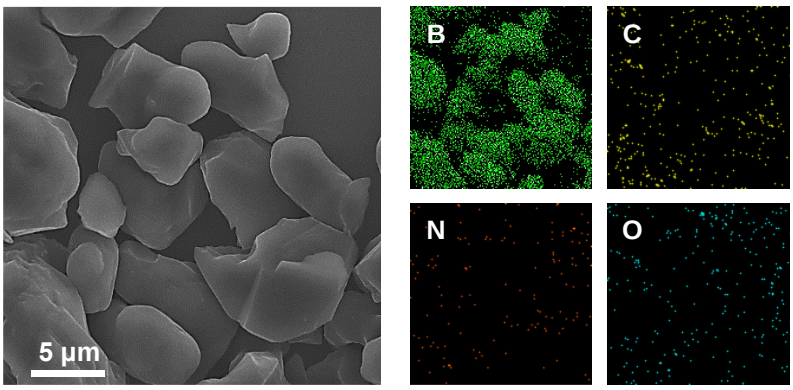

Fig. S5 Typical SEM image of Bulk B, corresponding elemental mapping images of B, C, N and O.

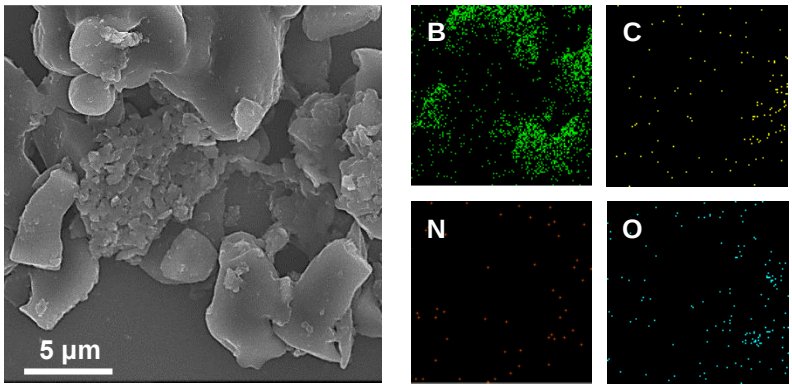

Fig. S6 Typical SEM image of BNS, corresponding elemental mapping images of B, C, N and O.

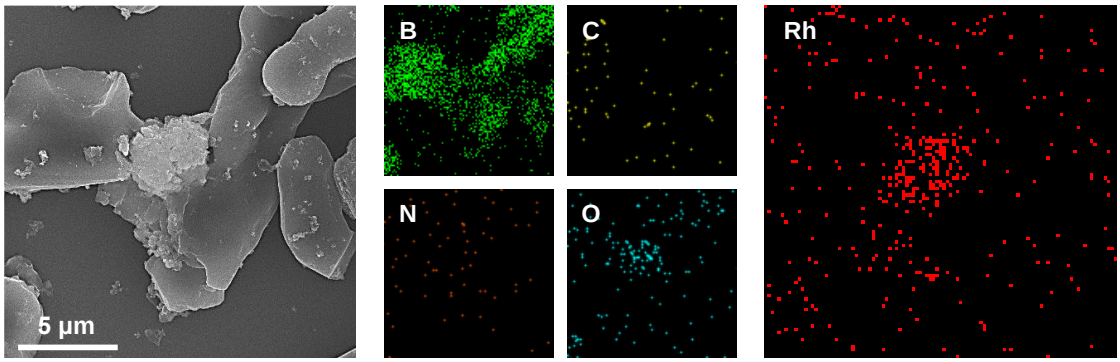

Fig. S7 Typical SEM image of Rh NP@BNS, corresponding elemental mapping images of B, C, N, O and Rh.

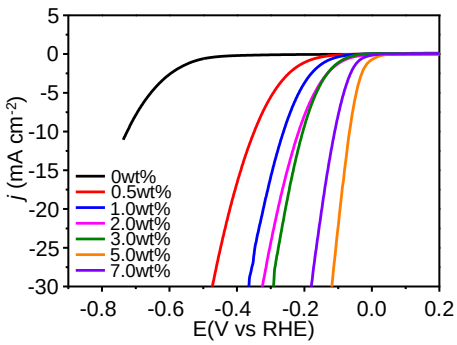

Fig. S8 HER polarization curves of x-Rh NP@BNS (x=0, 0.5, 1.0, 2.0, 3.0, 5.0, 7.0, x represents the mass percentage of Rh added during the preparation process) performed in 0.5 M H_2SO_4 electrolyte.

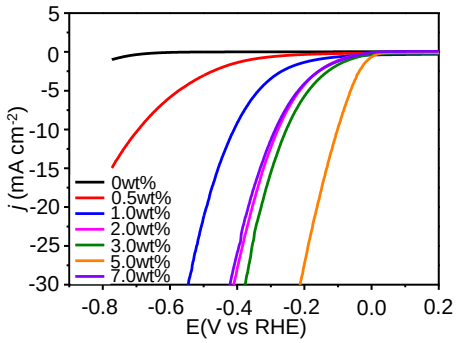

Fig. S9 HER polarization curves of x-Rh NP@BNS (x=0, 0.5, 1.0, 2.0, 3.0, 5.0, 7.0, x represents the mass percentage of Rh added during the preparation process) performed in 1.0 M KOH electrolyte.

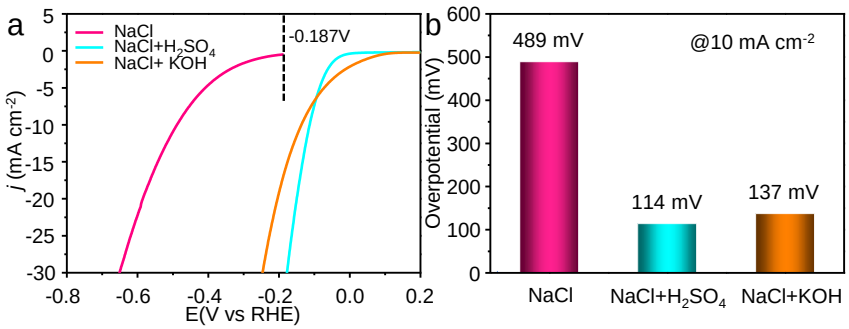

Fig. S10 a HER LSV curves of Rh NP@BNS performed in 1.0 M NaCl, 1.0 M NaCl+0.5 M H_2SO_4, and 1.0 M NaCl+1.0 M KOH electrolyte. **b** Comparison of the overpotentials at 10 mA cm^2.

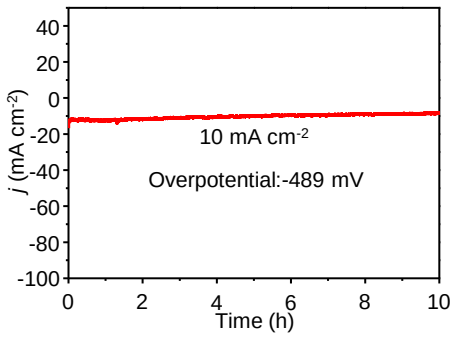

Fig. S11. Time dependence of current density at 489 mV versus RHE in 1.0 M NaCl electrolyte.

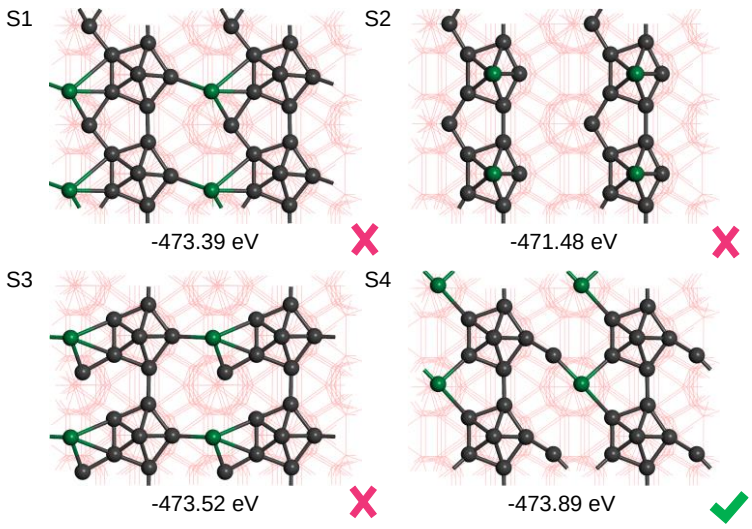

Fig. S12 Static optimization structure of Pt@B(104).

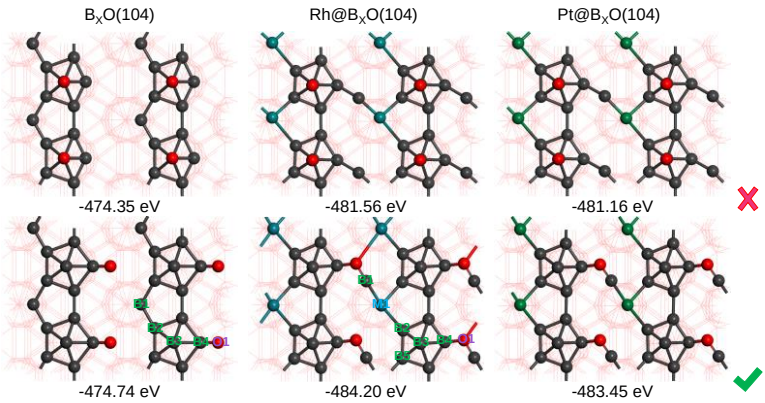

Fig. S13 Static optimization of surface oxidation structures of $B_xO(104)$, Rh@$B_xO(104)$ and Pt@$B_xO(104)$.

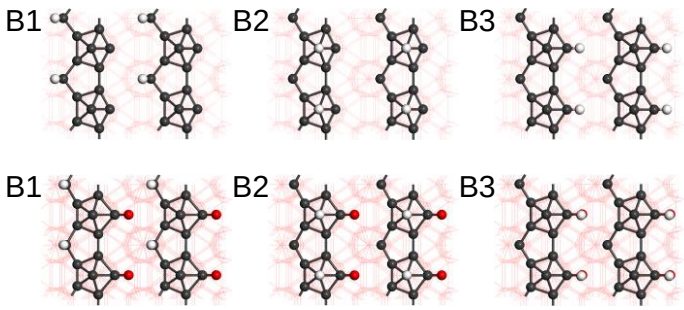

Fig. S14 Geometries Structures for the H adsorption of B(104) and $B_xO(104)$ Surface.

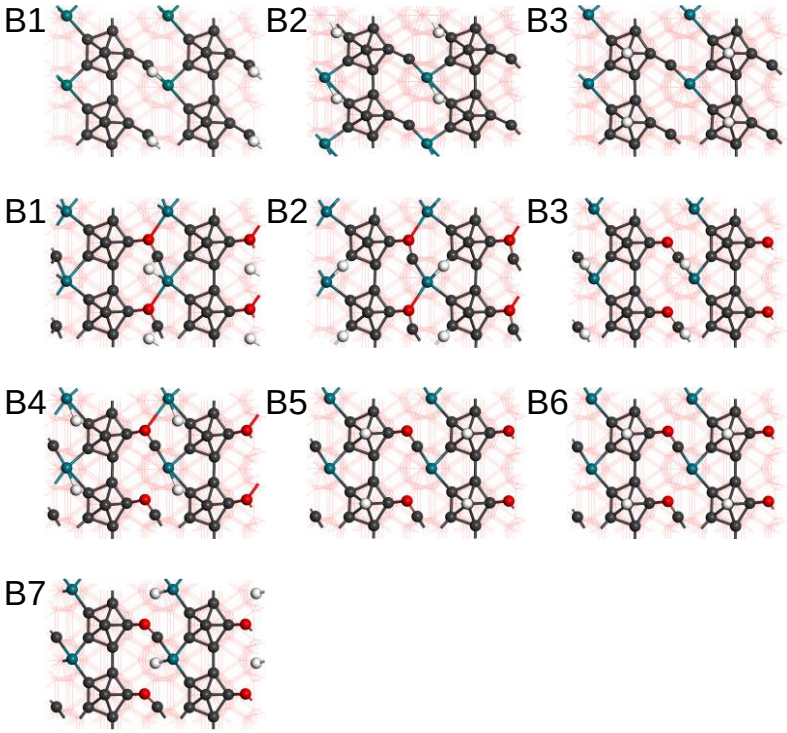

Fig. S15 Geometries Structures for the H adsorption of Rh@B(104) and Rh@B_xO(104) Surface.

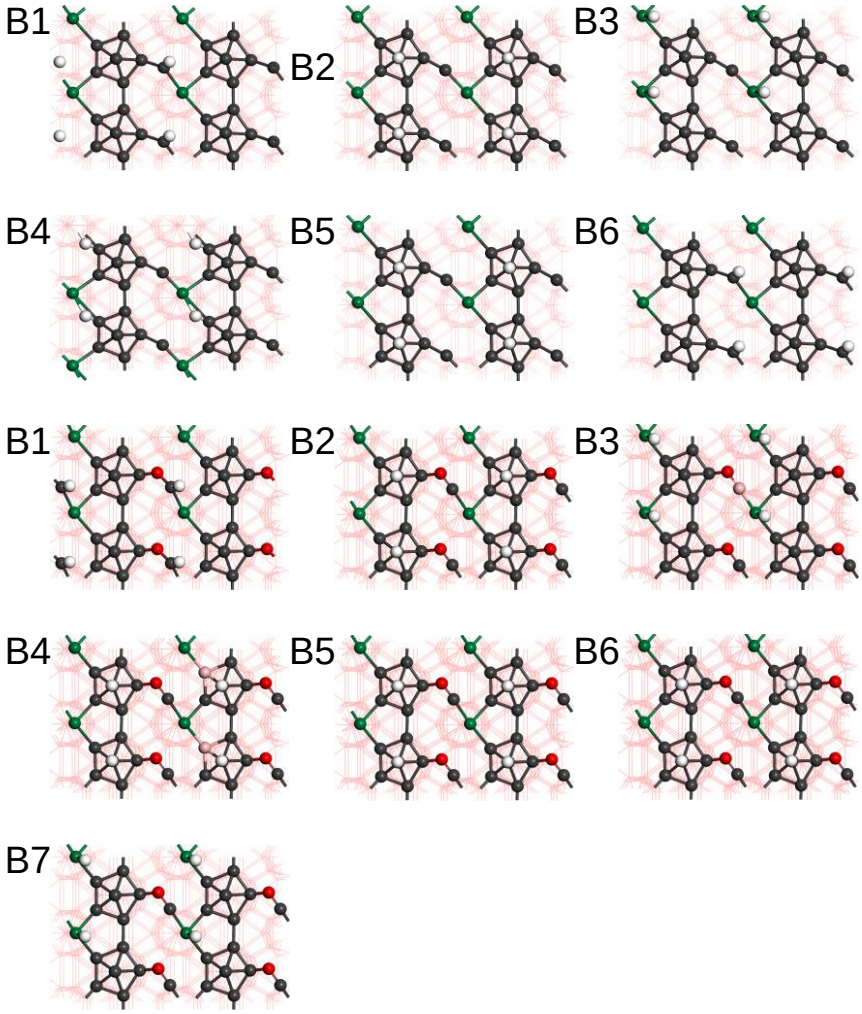

Fig. S16 Geometries Structures for the H adsorption of Pt@B(104) and Pt@B_xO(104) Surface.

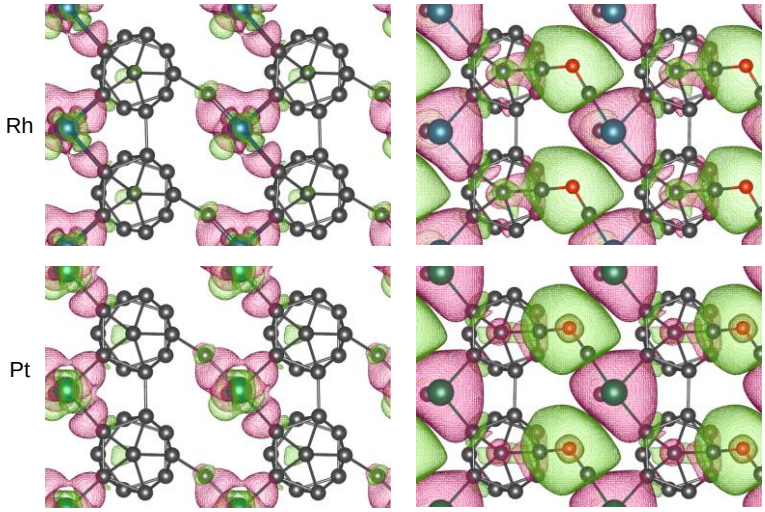

Fig. S17 Isosurface of charge density difference ($\Delta\rho$) for Rh@B_xO(104), Pt@B_xO(104).

Table S1 The total Rh content of the deposition was obtained by ICP-oes test.

Element	Weight/g	Volume/mL	Dilution factor	Instrument Readings mg/L	Concentration mg/kg	Percentage wt%
Rh	0.0244	50	1	5.4157	11097.6876	1.11

Table S2 DFT-calculated ΔGH* of various Geometries Structures for the H adsorption of B(104), B_xO(104), M@B(104) and M@B_xO(104) Surface (M=Rh, Pt).

Doping structures	**Sites**	**E_{DFT}**	**Ox**	**Sites**	**E_{DFT}**
B(104)	1	**-470.91**	B_xO(104)	1	**-478.30**
	2	-472.49		2	-478.97
	3	-472.64		3	-480.22
Rh@B(104)	1	**-478.56**	Rh@B_xO(104)	1	-487.85
	2	-469.99		2	-487.02
	3	-478.56		3	-487.81
	4	-471.27		4	-487.95
	5	-479.60		5	-489.00
	6	-		6	-
	-	-		7	-487.29
Pt@B(104)	1	**-478.22**	Pt@B_xO(104)	1	**-487.39**
	2	-		2	-
	3	-477.44		3	-486.81
	4	-477.65		4	-
	5	-479.19		5	-488.84
	6	-		6	-
	-	-		7	-486.81

Table S3 DFT-calculated binding energy (BE) of various B_{32} doping structures, spin magnetic moment (μ) of single metal atoms were also listed.

Doping structures	BE(eV)	μ(μ_B)
Ti	-3.45	4.00
Mn	-1.98	5.00
Fe	-3.22	4.00
Ni	-3.85	2.00
Cu	-2.03	1.00
Mo	-2.98	6.00
Pt	-3.49	2.00
Rh	-4.17	1.00
Pd	-1.68	0.00

Table S4 Comparison of HER activities of catalysts in acidic electrolytes (0.5 M H_2SO_4)

Catalyst	Rh metal content (wt%)	Rh nanoparticle size (nm)	Overpotential at 10 mA cm^{-2} (mV)	Tafel slope (mV dec^{-1})	Reference
Rh NP@BNS	1.11	~3	66	56	This work
Rh-Ag/SiNW	2.3	12.3	120	51	[S1]
Rh-Au/SiNW	2.2	15.8	62	24	[S2]
rGO/CoP-Rh	NA	12.86	72	43	[S3]
Rh/SWNTs	6.1	~2	25	20	[S4]
$MoSe_2$/Rh	NA	~8	192	47	[S5]
Rh/F-graphene	9.2	9.39	46	30	[S6]
Rh-CN	4.2	3.4	13	25	[S7]
Rh/Ni@NCNTs	2.84	1.92	45	37.2	[S8]
B-RhFe alloy	~18.29	4.01	25	32	[S9]
Rh-Rh_2P@C	NA	3.4	24	35.8	[S10]

Table S5 Comparison of HER activities of catalysts in alkaline electrolytes (1.0 M KOH)

Catalyst	Rh metal content (wt%)	Rh nanoparticle size (nm)	Overpotential at 10 mA cm^{-2} (mV)	Tafel slope (mV dec^{-1})	Reference
Rh NP@BNS	1.11	3	101	75	This work
rGO/CoP-Rh	NA	12.86	155	101	[S3]
$MoSe_2$/Rh	NA	~8	173	NA	[S5]
Rh/SWNTs	6.1	~2	25	20	[S4]
Rh–$MoSe_2$ nanoflowers	8.2	2.5	73	118	[S11]
Rh-CN	4.2	3.4	55	44	[S7]
Rh/Ni@NCNTs	2.84	1.92	45	37.2	[S8]
Rh-Rh_2P@C	NA	3.4	37	32	[S10]
P-Rh/C	12.57	1.98	11	71.4	[S12]
Rh/N-CBs	3.5	~1.4	77	74.16	[S13]
Rh NSs	NA	18.4	43	107.2	[S14]

Supplementary References

[S1] B. Jiang, Y. Sun, F. Liao, W. Shen, H. Lin, H. Wang, M. Shao, Rh–Ag–Si ternary composites: highly active hydrogen evolution electrocatalysts over Pt–Ag–Si, J. Mater. Chem. A 5 (2017) 1623-1628.

[S2] B. Jiang, L. Yang, F. Liao, M. Sheng, H. Zhao, H. Lin, M. Shao, A stepwise-designed Rh-Au-Si nanocomposite that surpasses Pt/C hydrogen evolution activity at high overpotentials, Nano Res. 10 (2017) 1749-1755.

[S3] H. Zheng, X. Huang, H. Gao, W. Dong, G. Lu, X. Chen, G. Wang, Decorating cobalt phosphide and rhodium on reduced graphene oxide for high-efficiency hydrogen evolution reaction, J. Energy Chem. 34 (2019) 72-79.

[S4] W.Q. Zhang, X. Zhang, L. Chen, J.Y. Dai, Y. Ding, L.F. Ji, J. Zhao, M. Yan, F.C. Yang, C.R. Chang, S.J. Guo, Single-Walled Carbon Nanotube Induced Optimized Electron Polarization of Rhodium Nanocrystals To Develop an Interface Catalyst for Highly Efficient Electrocatalysis, Acs Catal. 8 (2018) 8092-8099.

[S5] M.D. Sharma, C. Mahala, M. Basu, Nanosheets of $MoSe_2$@M (M=Pd and Rh)

function as widespread pH tolerable hydrogen evolution catalyst, J. Colloid Interface Sci. 534 (2019) 131-141.

[S6] W. Shen, L. Ge, Y. Sun, F. Liao, L. Xu, Q. Dang, Z. Kang, M. Shao, Rhodium Nanoparticles/F-Doped Graphene Composites as Multifunctional Electrocatalyst Superior to Pt/C for Hydrogen Evolution and Formic Acid Oxidation Reaction, ACS Appl. Mater. Interfaces 10 (2018) 33153-33161.

[S7] B. Jiang, A. Huang, T. Wang, Q. Shao, W. Zhu, F. Liao, Y. Cheng, M. Shao, Rhodium/graphitic-carbon-nitride composite electrocatalyst facilitates efficient hydrogen evolution in acidic and alkaline electrolytes, J. Colloid Interface Sci. 571 (2020) 30-37.

[S8] Q. Wang, B. Xu, C. Xu, Y. Wang, Y. Zhang, J. Wu, G. Fan, Ultrasmall Rh nanoparticles decorated on carbon nanotubes with encapsulated Ni nanoparticles as excellent and pH-universal electrocatalysts for hydrogen evolution reaction, Appl. Surf. Sci. 495 (2019) 143569.

[S9] L. Zhang, J. Lu, S. Yin, L. Luo, S. Jing, A. Brouzgou, J. Chen, P.K. Shen, P. Tsiakaras, One-pot synthesized boron-doped RhFe alloy with enhanced catalytic performance for hydrogen evolution reaction, Appl. Catal. B-Environ. 230 (2018) 58-64.

[S10] F. Luo, L. Guo, Y. Xie, J. Xu, W. Cai, K. Qu, Z. Yang, Robust hydrogen evolution reaction activity catalyzed by ultrasmall Rh–Rh_2P nanoparticles, J. Mater. Chem. A 8 (2020) 12378-12384.

[S11] Y. Zhao, C. Yang, G. Mao, J. Su, G. Cheng, W. Luo, Ultrafine Rh nanoparticle decorated $MoSe_2$ nanoflowers for efficient alkaline hydrogen evolution reaction, Inorg. Chem. Front. 5 (2018) 2978-2984.

[S12] L. Su, Y. Zhao, F. Yang, T. Wu, G. Cheng, W. Luo, Ultrafine phosphorus-doped rhodium for enhanced hydrogen electrocatalysis in alkaline electrolytes, J. Mater. Chem. A 8 (2020) 11923-11927.

[S13] N. Jia, Y. Liu, L. Wang, P. Chen, X. Chen, Z. An, Y. Chen, 0.2 V Electrolysis Voltage-Driven Alkaline Hydrogen Production with Nitrogen-Doped Carbon Nanobowl-Supported Ultrafine Rh Nanoparticles of 1.4 nm, ACS Appl. Mater.

Interfaces 11 (2019) 35039-35049.

[S14] N. Zhang, Q. Shao, Y. Pi, J. Guo, X. Huang, Solvent-Mediated Shape Tuning of Well-Defined Rhodium Nanocrystals for Efficient Electrochemical Water Splitting, Chem. Mater. 29 (2017) 5009-5015.